Taylor & Francis
Taylor & Francis Group

Journal of Macromolecular Science, Part A
Pure and Applied Chemistry

ISSN: 1060-1325 (Print) 1520-5738 (Online) Journal homepage: www.tandfonline.com/journals/lmsa20

Preparation and characterization of polymeric micelles from uracil-containing amphiphilic copolymer for donepezil delivery

Ayça Erkent, Gizem İğdeli, Rabia Sare Yanıkoğlu & Binnur Aydogan Temel

To cite this article: Ayça Erkent, Gizem İğdeli, Rabia Sare Yanıkoğlu & Binnur Aydogan Temel (2025) Preparation and characterization of polymeric micelles from uracil-containing amphiphilic copolymer for donepezil delivery, Journal of Macromolecular Science, Part A, 62:12, 1316-1325, DOI: 10.1080/10601325.2025.2584621

To link to this article: https://doi.org/10.1080/10601325.2025.2584621

JOURNAL OF MACROMOLECULAR SCIENCE, PART A: PURE AND APPLIED CHEMISTRY
2025, VOL. 62, NO. 12, 1316–1325
https://doi.org/10.1080/10601325.2025.2584621

Preparation and characterization of polymeric micelles from uracil-containing amphiphilic copolymer for donepezil delivery

Ayça Erkent[a]*, Gizem İğdeli[b]*, Rabia Sare Yanıkoğlu[c], and Binnur Aydogan Temel[a]

[a]Department of Pharmaceutical Chemistry, Faculty of Pharmacy, Bezmialem Vakif University, Istanbul, Turkey; [b]Department of Biotechnology, Institute of Health Sciences, Bezmialem Vakif University, Istanbul, Turkey; [c]Department of Biochemistry, Faculty of Pharmacy, Bezmialem Vakif University, Istanbul, Turkey

ABSTRACT

Alzheimer's disease (AD) remains one of the most challenging neurodegenerative disorders, and the development of advanced drug delivery systems is critical to improve the therapeutic potential of existing treatments. In this study, uracil functionalized amphiphilic block copolymers were designed and synthesized *via* RAFT polymerization to prepare polymeric micelles as nanocarriers for donepezil (DNP) delivery. The successful synthesis of the monomer and copolymer was confirmed by spectroscopic and chromatographic techniques. The self-assembled micelles exhibited uniform nanoscale sizes, spherical morphology, and high thermodynamic stability due to uracil-mediated hydrogen bonding within the core. DNP was successfully encapsulated into the micelles, and *in vitro* release studies revealed a sustained and controlled drug release profile. Biological evaluations demonstrated that drug-loaded micelles preserved the acetylcholinesterase (AChE) inhibitory activity of DNP while reducing the inherent cytotoxicity observed in the free drug and empty micelles. These results highlight the potential of uracil-containing polymeric micelles as a promising nanocarrier platform for DNP delivery, offering improved stability, favorable release behavior, and enhanced biocompatibility, thereby contributing to the development of safer and more effective therapeutic strategies for AD.

GRAPHICAL ABSTRACT

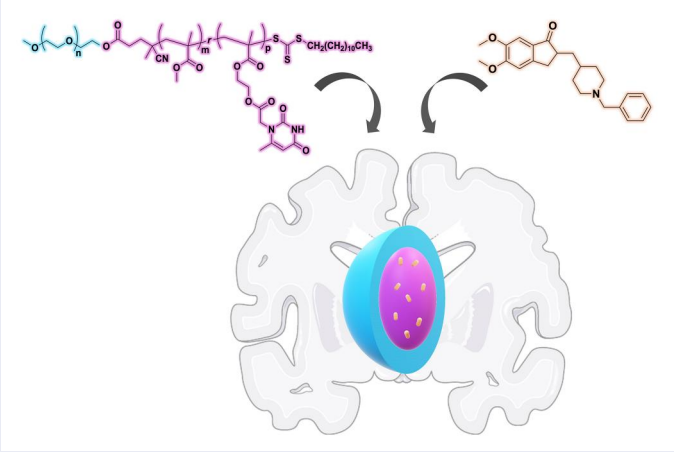

ARTICLE HISTORY
Received October 2025
Accepted October 2025

KEYWORDS
Alzheimer's disease; RAFT polymerization; 6-methyluracil; donepezil; acetylcholinesterase

1. Introduction

Alzheimer's disease (AD) is a progressive neurodegenerative disorder that affects more than 35 million people worldwide.[1] It is clinically characterized by progressive memory loss, apraxia, anomia, confusion, and decline in daily functional abilities. Neuropathological hallmarks of AD include amyloid-rich senile plaques, neurofibrillary tangles, and widespread neuronal degeneration.[2,3] These changes lead to executive dysfunction, significant cognitive impairment, and behavioral alterations, ultimately reducing patients' quality of life and life expectancy to approximately 7–10 years after diagnosis.[4,5] Two main hypotheses have been proposed to explain the molecular mechanisms underlying AD: the amyloid cascade hypothesis and the cholinergic hypothesis. The amyloid cascade hypothesis suggests that abnormal processing of amyloid precursor protein (APP) leads to

CONTACT Binnur Aydogan Temel baydogan@bezmialem.edu.tr Department of Pharmaceutical Chemistry, Faculty of Pharmacy, Bezmialem Vakif University, Fatih, Istanbul, 34093, Turkey.
*These authors equally contributed to this work.

Supplemental data for this article can be accessed online at https://doi.org/10.1080/10601325.2025.2584621.

amyloid-β (Aβ) production, aggregation, and toxicity in the brain.[6] The cholinergic hypothesis emphasizes that the cognitive and behavioral impairments in AD result from insufficient stimulation of cholinergic synapses due to reduced acetylcholine levels.[6] Indeed, a marked decline in choline acetyltransferase activity in cortical regions has been linked to cholinergic dysfunction. For this reason, acetylcholinesterase inhibitors (AChEIs) remain the most widely used therapeutic agents to alleviate AD symptoms by enhancing cholinergic neurotransmission.[7,8] Among them, donepezil is a reversible, noncompetitive inhibitor of acetylcholinesterase that provides long-lasting central cholinesterase inhibition with limited peripheral effects.[9] In addition to improving cholinergic transmission, donepezil (DNP) has been reported to exhibit neuroprotective effects by reducing neuroinflammation.[10] However, its therapeutic efficacy is limited by drawbacks such as gastrointestinal side effects, rapid metabolism, broad tissue distribution, and the need for daily dosing, which decreases patient compliance.[11] Therefore, developing advanced drug delivery systems to improve the bioavailability, stability, and targeted delivery of DNP is of considerable importance.[12–20]

Nanotechnology-based systems, particularly polymeric nanocarriers, have emerged as promising strategies to overcome the limitations of conventional drug formulations. Their small size, tunable surface properties, and high surface area-to-volume ratio allow improved solubility, extended systemic circulation, and controlled release of drugs.[21–23] Polymeric micelles, self-assembled from amphiphilic block copolymers, are especially attractive due to their core–shell architecture, biocompatibility, and ability to protect hydrophobic drugs while prolonging circulation time under physiological conditions.[24–26] These features make them suitable for central nervous system drug delivery. In this context, our research group has previously investigated polymeric micelles as nanocarriers for DNP. In our earlier work, we demonstrated the feasibility of PEG-based micelles for drug encapsulation and delivery.[27] In a subsequent study, we showed that folic acid functionalization further improved cellular uptake and permeability across the blood–brain barrier.[28]

Building on these findings, the present study explores the incorporation of uracil-derived functionalities to enhance micellar stability and therapeutic performance. For this purpose, a methacrylate monomer derived from 6-methyluracil, a close analogue of uracil and 5-methyluracil, was synthesized. Beyond its structural suitability, 6-methyluracil has been widely used in pharmaceutical formulations for its biological activities, including regulation of lipid peroxidation, promotion of wound healing, and as a component of therapeutic complexes investigated for conditions such as ischemia, type I diabetes, stroke, and neurodegenerative diseases including AD and Parkinson's disease.[29] The synthesized monomer was polymerized *via* RAFT polymerization to obtain the amphiphilic block copolymer PEG-*b*-P(MMA-*r*-UMA). Polymeric micelles were subsequently prepared, and DNP was successfully encapsulated. The micelles were characterized in terms of size and stability, and their *in vitro* drug release, cytotoxicity, and anticholinesterase activity were systematically evaluated using the human neuroblastoma SH-SY5Y (CRL-2266) cell line. This study aims to combine the therapeutic potential of DNP with the stabilizing and bioactive properties of uracil derivatives to develop an improved nanocarrier system for Alzheimer's therapy.

2. Materials and methods

2.1. Materials

Bromoacethyl bromide (Sigma-Aldrich), 6-methyluracil (Aldrich), poly(etyhlene glycol) methyl ether (mPEG, M_n= 5000, Aldrich), donepezil hydrochloride (Thermo Scientific), triethylamin (TEA, Sigma-Aldrich), tetrabutylammonium iodide (TBAI, Sigma-Aldrich), sodium bicarbonate ($NaHCO_3$, Merck) potassium carbonate (K_2CO_3, Merck), sodium sulfate anhydrous (Na_2SO_4, Merck), magnesium sulfate anhydrous ($MgSO_4$, VWR), 4-cyano-4-[(dodecylsulfanylthiocarbonyl)sulfanyl]pentanoic acid (CDTP, 97%, Strem Chemicals), 4-(dimethylamino) pyridine (DMAP, Merck), *N*,*N*'-dicyclohexyl carbodiimide (DCC, Alfa Aesar), 5,5′-dithiobis(2-nitrobenzoic acid) (DTNB, ≥98%, Sigma-Aldrich), ethyl acetate (Merck), n-hexane (Emplura), methanol (CH_3OH, Merck), diethyl ether (Chem-Lab), toluene (Merck) and tetrahydrofuran (THF, Merck) were used as received. Dichloromethane (DCM, Merck) and *N*,*N*-dimethylformamide (DMF,+99.8%, Alpha Aesar) were used after dried with 4 Å sized molecular sieve. 2,2′-Azobis(2-methylpropionitrile) (AIBN, Aldrich) was used after crystallization from methanol. Methyl methacrylate (MMA, Aldrich) and 2-hydroxyethyl methacrylate (HEMA, Aldrich) were used by passing through a basic alumina column. The electric eel acetylcholinesterase (AChE, Type-VI-S, EC 3.1.1.7, 425.84 U/mg, Sigma) were purchased from Sigma. The macro-RAFT agent was synthesized using a procedure described in our previous study.[27]

2.2. Instrumentation

Fourier transform infrared (FTIR) spectra were recorded in ALPHA Bruker spectrometer with platinum-ATR accessory (ZnSe crystal). ^{1}H NMR and ^{13}C NMR measurements were taken at 500 MHz Bruker NMR device by using $CDCl_3$ solvent. Gel permeability chromatography (GPC) measurements were taken by using Viscotek GPCmax and 2001 Autosampler system consisting of a pump and Viscotek and 3580 refractive index (RI) detector. Three Viscotek GPC columns (T3000, LT4000L and LT5000L) connected in series (inner diameter 7.8 mm, length 300 mm) and one Viscotek guard column (CLM3008, inner diameter 4.6 mm, length 10 mm) were used. The measurements were taken at a flow rate of 1.0 mL/min at 35 °C and THF was used as the solvent. The detector was calibrated with PS standards with narrow molecular weight distribution and the data were analyzed using Viscotek OmniSEC 4.7.0 software. During micelle formation, injections were performed using syringes with an inner diameter of 19.23 mm on a Sujipuli Technology NE-1600 six-channel programmable syringe

pump at a flow rate of 0.5 mL/min. The average particle size and particle size distributions of the micelles were determined with a measurement angle of 173° in distilled water (H_2O) using a Malvern NanoZSP dynamic light scattering (DLS) spectrometer device at a wavelength of 633 nm and 25 °C. The transmission electron microscopy (TEM) micrographs were obtained using a JEOL JEM-2100PLUS transmission electron microscope. The samples were prepared by casting the micellar solution onto a copper grid. The grids were dried by air and then negatively stained with uranyl acetate. Polymer micelles were lyophilized using a CHRIST Alpha 3–4 LSCbasic freze-dry system. BioTek microplate reader (SynergyTM H1) was used for determination of drug encapsulation efficiency, drug release studies and also activity assay.

2.3. Synthesis of 2-(2-bromoacetoxy)ethyl methacrylate

Bromoacetyl bromide (2.686 mL, 0.03074 mol) was added dropwise in an ice bath to a solution of HEMA (4.0 g, 0.03074 mol) and TEA (4.712 mL, 0.03381 mol) in dry DCM (92 mL) under a nitrogen atmosphere. The reaction mixture was stirred at room temperature for 48 h. Unreacted bromoacetyl bromide was then quenched with methanol (2 mL), and stirring was continued for an additional 30 min. The solution was transferred into saturated aqueous $NaHCO_3$ (50 mL) and extracted once, followed by five extractions with distilled water (5 × 55 mL). The combined organic layer was dried over anhydrous $MgSO_4$, filtered, concentrated using a rotary evaporator, and further dried in a fume hood to yield a brown oil. Purification by column chromatography (20% ethyl acetate in hexane) afforded a colorless oil (3.43 g, 44.5%).

2.4. Synthesis of 2-(2-(6-methyluracil-1-yl)acetoxy)ethyl methacrylate (UMA)

Anhydrous K_2CO_3 (1.96 g, 0.0142 mol) was added to a solution of 6-methyluracil (1.788 g, 0.0142 mol) in dry DMF (90 mL) and stirred for 30 min. TBAI (0.3324 g, 0.8762 mmol) was then added, and the mixture was cooled in an ice bath. 2-(2-Bromoacetoxy)ethyl methacrylate (2.0 g, 7.966 mmol) was added dropwise, and the reaction was carried out under a nitrogen atmosphere at room temperature for 48 h. The mixture was filtered, and the filtrate was concentrated using a rotary evaporator. The resulting solid was dissolved in DCM (65 mL) to remove excess 6-methyluracil and filtered. The DCM solution was then extracted with distilled water four times (4 × 55 mL). The organic layer was collected, dried over anhydrous Na_2SO_4, filtered, concentrated by rotary evaporation, and further dried in a fume hood. The obtained solid was washed with hexane to remove residual DMF and dried in the fume hood. Finally, the solid was dissolved in DCM (2 mL) and further purified by column chromatography (2% MeOH in DCM). The purified product was concentrated by rotary evaporation and dried in a fume hood (1.156 g, 42.6%).

2.5. Synthesis of poly(ethylene glycol) methyl ether-b-poly[methyl methacrylate-r-(2-(2-(6-methyluracil-1-yl)acetoxy)ethyl methacrylate)] (PEG-b-P(MMA-r-UMA)) by RAFT polymerization

UMA (0.19 g, 0.00065 mol), MMA (1.3 mL, 0.012271 mol), macro-RAFT agent (0.347 g, 0.064588 mmol) and AIBN (0.0035 g, 0.021314 mmol) were dissolved in 6 mL dry toluene in a Schlenk tube. After degassing the solution by three freeze–pump–thaw cycles, it was brought to room temperature and then stirred at 70 °C for 18 h. At the end of this period the reaction was stopped by immediate cooling of the flask. The polymer was precipitated in cold methanol, filtered and dried under vacuum at room temperature.

2.6. Preparation of polymeric micelles

Polymeric micelles were prepared using the dialysis membrane method. PEG-*b*-P(MMA-*r*-UMA) copolymer (0.01 g) was dissolved in DMF (2 mL) and stirred at room temperature for 1 h. Distilled water (8 mL) was then added dropwise using an injection pump at a rate of 0.5 mL/min. The resulting solution was stirred overnight at room temperature and subsequently transferred into a dialysis membrane (MWCO = 6–8 kDa) for dialysis against distilled water for 24 h.

2.7. Preparation of donepezil (DNP) loaded polymeric micelles

Donepezil·HCl was stirred with TEA (2 molar equivalents) in DMF (2 mL) overnight to remove HCl and obtain free donepezil. Polymeric micelles were then prepared using the dialysis method. PEG-*b*-P(MMA-*r*-UMA) copolymer (0.01 g) was dissolved in DMF (2 mL) and stirred at room temperature for 1 h. Distilled water (8 mL) was subsequently added dropwise using an injection pump at a rate of 0.5 mL/min. The resulting solution was stirred overnight at room temperature and transferred into a dialysis membrane (MWCO = 6–8 kDa) for dialysis against distilled water for 24 h.

2.8. Determination of critical micelle concentration (CMC)

The critical micelle concentration (CMC) of the polymeric micelles was determined using the fluorescent dye solubilization method with pyrene as a probe. Pyrene (5 mg) was dissolved in acetone (5 mL), and 10 µL of this solution was transferred into Eppendorf tubes. Acetone was evaporated under vacuum at room temperature overnight. Polymer micelle solutions (1 mL) with concentrations ranging from 1×10^{-4} to 1 mg/mL were added to the pyrene-containing tubes and sonicated for 2 min. The samples were kept in the dark overnight and then transferred into a 96-well plate for fluorescence measurements. Excitation was performed at 334 nm, and the emission intensities at 371 nm (I_1) and 391 nm (I_3) were recorded. The CMC of the micelles was

estimated from the plot of the I_3/I_1 ratio versus the logarithm of polymer concentration.

2.9. Drug loading content (DLC) and drug loading efficiency (DLE) assay

DNP loaded polymer micelles were dissolved in DMSO (1 mL) and kept in dark at room temperature overnight. The absorbance value at the 312 nm was measured using UV/Vis microplate reader. DLC and DLE were calculated according to the following equations:

$$\text{Drug loading content } (\%) = \frac{\text{Weight of loaded drug}}{\text{Weight of micelle}} \text{ x } 100$$

$$\text{Drug loading efficiency } (\%) = \frac{\text{Weight of loaded drug}}{\text{Weight of feeded drug}} \text{ x } 100$$

2.10. In vitro *drug release assay*

The release of DNP was evaluated using the dialysis method. DNP-loaded micelles (1 mg/mL) were placed in a dialysis bag and incubated in PBS (20 mL, pH 7.4) containing Tween® 80 (2% v/v) at 37 °C with stirring at 100 rpm. At predetermined time intervals (0, 1, 2, 4, 6, and 8 h), 2 mL of the release medium was withdrawn and replaced with an equal volume of fresh medium. The concentration of DNP in the collected samples (each in triplicate) was determined from a calibration curve using UV absorbance at 312 nm. The calibration curve was constructed by measuring the absorbance of standard DNP solutions prepared in PBS (2% Tween® 80 v/v) using a UV–Vis microplate reader.

2.11. Anticholinesterase activity assay

The acetylcholinesterase (AChE) inhibitory activities of the polmeric micelles were determined according to a literature method. The anticholinesterase activity of the polymeric micelles was assessed *in vitro* using the Ellman method.[30] Acetylthiocholine iodide was used as the substrate, and IC_{50} values were determined by constructing absorbance and/or inhibition (%) curves at different concentrations. For each inhibitor, the IC_{50} value was defined as the concentration required to inhibit 50% of the substrate's maximum biological response.

To measure anticholinesterase activity, 5,5′-dithiobis (2-nitrobenzoic acid) (DTNB) was employed. Sample and DNP solutions were prepared in n-propanol at a concentration of 100 µg/mL. Aliquots containing 150 µL of 100 mM phosphate buffer (pH 8.0), 10 µL of sample solution, and 20 µL of AChE solution (2.548×10^{-4} U/µL) were mixed and incubated at 25 °C for 15 min. The DTNB solution (10 µL) was prepared by mixing 1.0 mL of a solution containing 16 mg/mL DTNB and 7.5 mg/mL $NaHCO_3$ in phosphate buffer (pH 7.0) with 2.0 mL of pH 7.0 buffer and 4.0 mL of pH 8.0 buffer. The reaction was initiated by adding 10 µL of acetylthiocholine iodide (7.1 mM). Enzymatic activity was monitored by the formation of a yellow color, resulting from the reaction of DTNB with the thiolate anion released during hydrolysis of the substrate. Distilled water was used as the solvent control. Absorbance was measured at 412 nm using a UV–Vis microplate reader, and IC_{50} values were calculated accordingly.

2.12. Cell viability assay

Cell viability was assessed using a human neuroblastoma cell line (SH-SY5Y, CRL-2266). Cells were treated with the test compounds for 24 h, and viability was measured using the 3-(4,5-dimethylthiazol-2-yl)-2,5-diphenyltetrazolium bromide (MTT) assay. MTT was prepared at 5 mg/mL in phosphate-buffered saline (PBS) and added directly to the culture. After a 3 h incubation, metabolically active cells reduced tetrazolium to purple formazan crystals, which accumulated intracellularly and in the medium. The crystals were dissolved in the appropriate solvent, and absorbance was measured at 570 nm. The absorbance values were proportional to the number of viable cells.

Cells were cultured in DMEM-F12 (Gibco, Thermo Fisher Scientific, NY, USA) supplemented with 10% fetal bovine serum (FBS; Gibco) and 1% penicillin–streptomycin. Cultures were maintained at 37 °C in a humidified atmosphere of 5% CO_2 and 95% relative humidity. For cytotoxicity experiments, 5×10^3 cells were seeded into 96-well plates and allowed to attach for 24 h. The cells were then washed with PBS and treated with 100 µL of medium containing one of six different concentrations of the test compounds for 24 h. Experiments were performed in duplicate ($n = 2$) for each condition, with two independent biological replicates conducted on separate days. Data are presented as mean ± standard deviation. Cell passages 10 and 11 were used in all experiments to ensure consistency and minimize variability.

3. Results and discussion

3.1. Synthesis and characterization of 2-(2-(6-methyluracil-1-yl)acetoxy)ethyl methacrylate (UMA)

In order to introduce uracil functionality into the polymer backbone and enhance the stability of polymeric micelles through hydrogen bonding, the synthesis of 2-(2-(6-methyluracil-1-yl)acetoxy)ethyl methacrylate (UMA) was successfully carried out in two steps, as illustrated in Scheme 1. In the first step, HEMA was reacted with bromoacetyl bromide to yield 2-(2-bromoacetoxy)ethyl methacrylate. In the second step, the obtained intermediate was functionalized with 6-methyluracil, resulting in the target UMA monomer.[31]

The FTIR spectra of HEMA, 2-(2-bromoacetoxy)ethyl methacrylate, and UMA are presented in Figure 1. The spectrum of HEMA (a) shows the broad absorption band around 3400 cm^{-1}, corresponding to the hydroxyl stretching vibration. In the spectrum of 2-(2-bromoacetoxy)ethyl methacrylate (b), this hydroxyl band disappears, confirming the successful esterification of HEMA with bromoacetyl bromide.

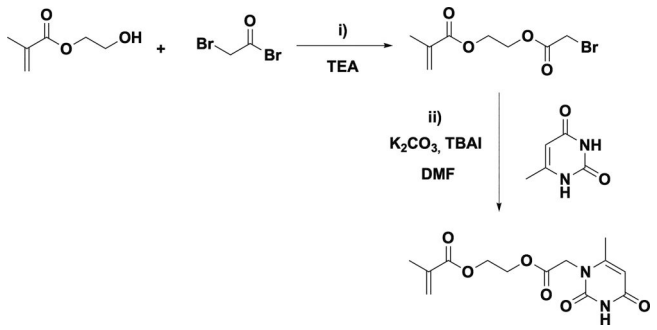

Scheme 1. Synthesis of (i) 2-(2-bromoacetoxy)ethyl methacrylate and (ii) 2-(2-(6-methyluracil-1-yl)acetoxy)ethyl methacrylate (UMA).

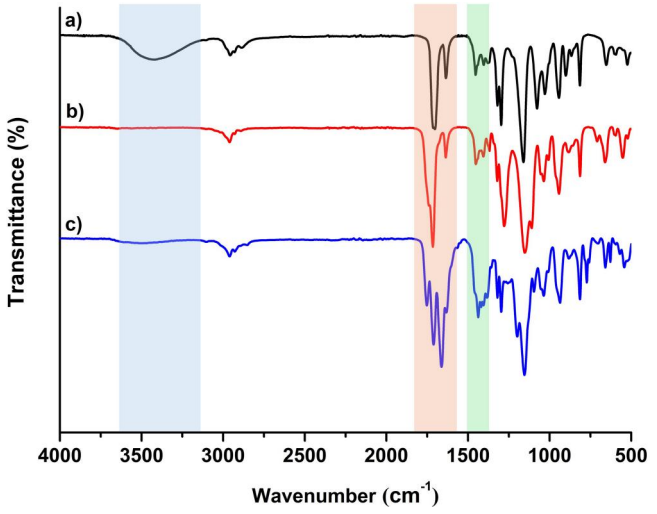

Figure 1. FTIR spectra of (a) 2-hydroxyethyl methacrylate (HEMA), (b) 2-(2-bromoacetoxy) ethyl methacrylate and (c) 2-(2-(6-methyluracil-1-yl) acetoxy) ethyl methacrylate (UMA).

In addition, the characteristic carbonyl stretching band is observed at ~1730 cm^{-1}, consistent with the presence of the ester group. In the spectrum of UMA (c), new absorption peaks associated with the uracil moiety are observed in the regions of 1680–1650 cm^{-1} (C=O stretching of uracil) and 1500–1450 cm^{-1} (C=C and C–N stretching), confirming the incorporation of 6-methyluracil into the structure.

The chemical structures of the intermediates and final product were further confirmed by ^{1}H NMR spectroscopy (Figure 2). The ^{1}H NMR spectrum of 2-(2-bromoacetoxy) ethyl methacrylate (A) shows the characteristic vinyl proton signals at δ 6.15 and 5.63 ppm (a and b), the methylene protons adjacent to the ester groups at δ 4.45 and 4.39 ppm (d and e), the methylene protons next to bromide at δ 3.87 ppm (f), and the methyl group of the methacrylate backbone at δ 1.95 ppm (c). These results are consistent with the expected structure of the intermediate. In the spectrum of UMA (B), additional peaks corresponding to the uracil unit appear. The aromatic proton of the uracil ring is observed at δ 8.75 ppm (m), while signals at δ 6.13 ppm (g), δ 5.62–5.60 ppm (a and b), and δ 4.61–4.39 ppm (f, d, e) confirm the retention of the methacrylate and linker moieties. The characteristic methyl group of 6-methyluracil is detected at δ 2.20 ppm (h) together with the methacrylate methyl resonance at δ 2.05 ppm (c). These data provide clear evidence for the successful attachment of 6-methyluracil to the methacrylate monomer.

In addition, the ^{13}C NMR spectra of both 2-(2-bromoacetoxy)ethyl methacrylate and UMA further confirmed their successful synthesis. The observed carbon resonances were in full agreement with the expected chemical structures, thereby providing complementary evidence to the ^{1}H NMR and FTIR analyses (Figures S1 and S2).

3.2. Synthesis and characterization of PEG-b-P(MMA-r-UMA)

PEG-*b*-P(MMA-*r*-UMA) amphiphilic copolymer was successfully synthesized by RAFT polymerization using the mPEG-based macro-RAFT agent, as previously reported in our earlier work.[27] The synthetic route is presented in Scheme 2. The copolymer design incorporated hydrophilic PEG blocks and a hydrophobic methacrylate block partially functionalized with UMA units, enabling the formation of micelles with uracil-mediated hydrogen bonding interactions.

The polymerization conditions and characterization results are summarized in Table 1. The copolymerization was conducted in toluene at 70 °C with a feed ratio of [UMA]/[MMA] = 5/95, using [M]:[RAFT]:[AIBN] = 200:1:0.33. After 18 h, a high monomer conversion of 82% was achieved, indicating the efficiency of the RAFT process. The theoretical number-average molecular weight ($M_{n,th}$) was calculated as 23750 g/mol, whereas the molecular weight determined by GPC ($M_{n,GPC}$) was 14940 g/mol with a narrow dispersity (M_w/M_n = 1.3) (Figure S3). The difference between the theoretical and GPC determined molecular weights can be attributed to the use of polystyrene standards in GPC calibration, which often underestimates the molecular weight of PEG-based block copolymers. The $M_{n,NMR}$ value determined by ^{1}H NMR (16590 g/mol) was in good agreement with the GPC results, further confirming successful polymerization under controlled conditions.

The successful synthesis of PEG-*b*-P(MMA-*r*-UMA) was confirmed by ^{1}H NMR spectroscopy. The spectrum (Figure 3) displayed characteristic peaks corresponding to each segment of the block copolymer. The methylene protons of the PEG repeating units (–O–CH_2–CH_2–O–) appeared as a strong, broad signal at δ 3.55–3.70 ppm (b), confirming the presence of the hydrophilic PEG block. The uracil unit was clearly identified by the downfield aromatic proton resonance at δ ~8.7 ppm (9), as well as the methyl substituent of 6-methyluracil at δ ~2.0 ppm (11). Signals corresponding to the methylene groups adjacent to oxygen and carbonyl groups in the UMA were observed at δ 4.8–4.0 ppm (6 and 7), further verifying successful incorporation of UMA moieties. The characteristic backbone signals of the methacrylate units were detected between δ 2.1–1.5 ppm (1, 4, 2 and 5), consistent with the aliphatic methylene and methyl groups of MMA units. In addition, the RAFT end-group alkyl chain was evidenced at δ ~2.0 ppm (i), confirming the retention of the RAFT agent during polymerization. Importantly, the absence of vinyl resonances (δ ~6.1 and 5.6 ppm) indicated complete conversion of the methacrylate double bonds, verifying successful polymerization.

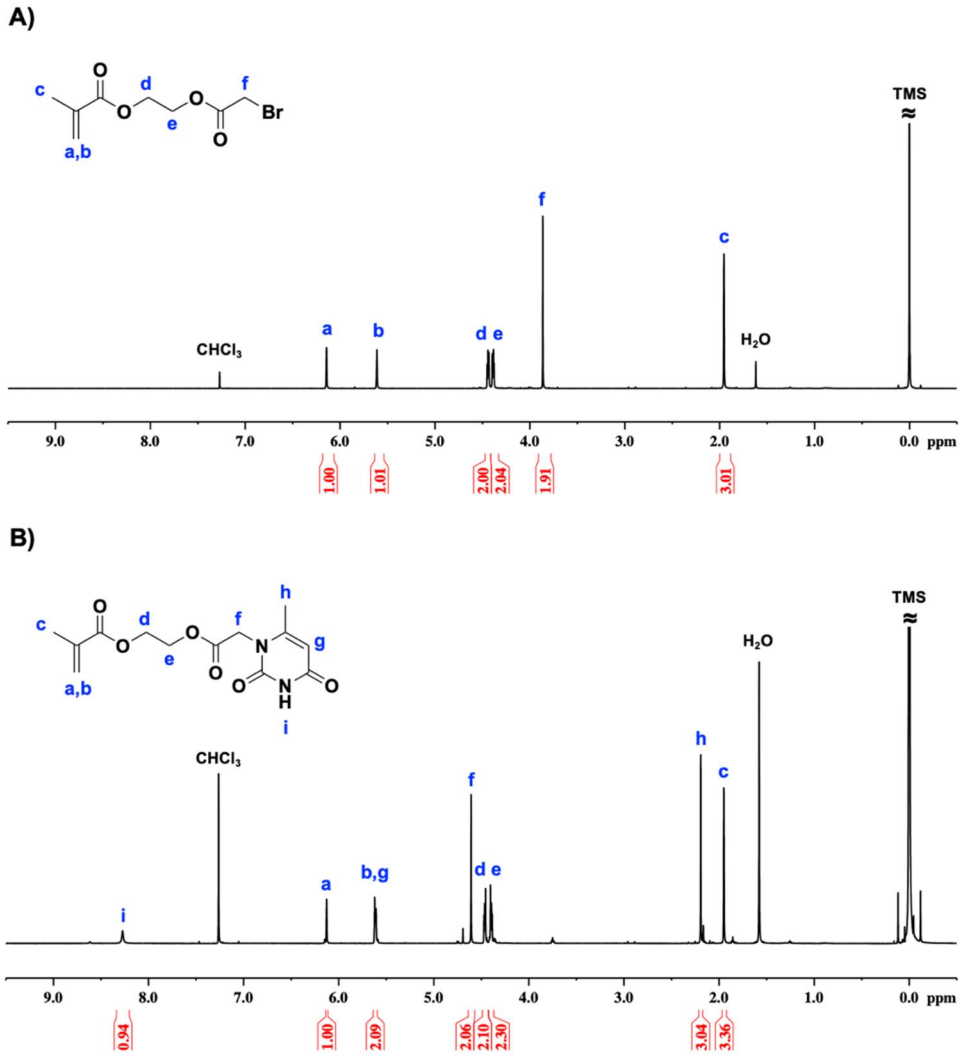

Figure 2. ^{1}H NMR spectra of the (a) 2-(2-bromoacetoxy)ethyl methacrylate and (b) 2-(2-(6-methyluracil-1-yl)acetoxy)ethyl methacrylate (UMA) in $CDCl_3$.

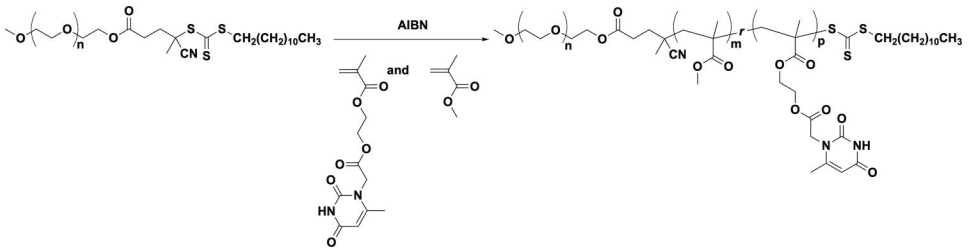

Scheme 2. Synthesis of PEG-*b*-P(MMA-*r*-UMA) by RAFT polymerization.

Table 1. Synthesis conditions and results of PEG-*b*-P(MMA-*r*-UMA).[a]

Polymer	Time (hour)	Conversion[b] (%)	$M_{n,th}$[b] (g/mol)	$M_{n,GPC}$[c] (g/mol)	M_w/M_n[c]	$M_{n,NMR}$[d] (g/mol)
PEG-*b*-P(MMA-*r*-UMA)	18	82	23750	14940	1.3	16590

[a][M]:[RAFT]:[AIBN] = 200:1:0.33. Toluen was used as solvent. Feed ratio [UMA]/[MMA] = 5/95.
[b]Calculated gravimetrically.
[c]Measured in THF by GPC.
[d]Determined by ^{1}H NMR.

The number of UMA units in the polymer was determined by comparing the relative integrals of the UMA signals with those of the RAFT agent. In a similar way, the total number of MMA units was calculated by evaluating the ratio of the MMA and RAFT agent signals. Based on these calculations, the polymer composition was estimated to contain approximately 4 UMA units and 83 MMA units.

3.3. Characterization of empty and drug loaded polymeric micelles

Dynamic light scattering (DLS) analysis was performed to evaluate the hydrodynamic diameters of the polymeric micelles prepared from PEG-*b*-P(MMA-*r*-UMA) and the corresponding drug loaded micelles (DPM). As shown in Table 2, the average particle size of the empty micelles (PM) was 67.1 ± 1.61 nm with a low polydispersity index (PDI = 0.168), indicating the formation of uniform and stable nanostructures. Upon loading with DNP, the particle size increased to 123.3 ± 0.92 nm while maintaining a narrow distribution (PDI = 0.153). The increase in size after drug loading can be attributed to the successful encapsulation of DNP molecules in the micellar core, which expands the hydrophobic domain. The low PDI values (<0.2) for both PM and DPM confirm the monodisperse nature of the micellar systems, a desirable feature for drug delivery applications.

The size distribution curve of DNP loaded micelles (Figure 4a) further supports these findings. The micelles exhibited a sharp unimodal distribution centered around ~120 nm, consistent with the average size obtained from DLS measurements. The absence of secondary peaks suggests that no aggregation or significant polydispersity occurred during micelle formation or drug encapsulation. The morphology of the DNP loaded micelles was investigated using transmission electron microscopy (TEM). As shown in Figure 4b, spherical micelles with well-defined structures were observed. The particle size observed by TEM was in good agreement with the DLS results, further validating the formation of nanoscale micellar assemblies. The spherical morphology and narrow size distribution demonstrate the capability of PEG-*b*-P(MMA-*r*-UMA) copolymers to self-assemble into stable nanostructures suitable for biomedical applications.

The CMC value of PEG-*b*-P(MMA-*r*-UMA) was calculated from the intersection point of the two fitted curves in the pyrene fluorescence plot (Figure S4). The CMC was determined to be 6×10^{-7} M, which is consistent with reported values for polymeric micelles (10^{-6}–10^{-7} M) and much lower than those of conventional small-molecule surfactant micelles (10^{-3}–10^{-4} M).[32] This low CMC indicates high thermodynamic stability of the micelles, suggesting that they remain intact even upon dilution under physiological conditions. The incorporation of 6-methyluracil units into the hydrophobic core is expected to further enhance micelle stability through additional hydrogen bonding interactions, thereby improving their potential as robust drug delivery carriers.

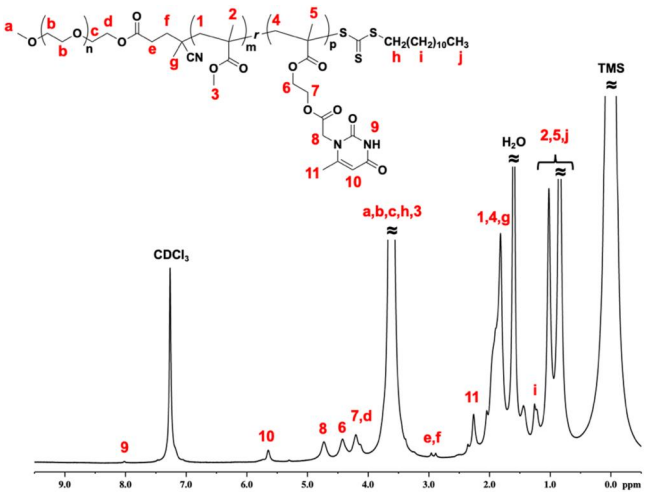

Figure 3. ^{1}H NMR spectrum of PEG-*b*-P(MMA-*r*-UMA) in $CDCl_3$.

Table 2. Dynamic light scattering (DLS) results of empty and drug loaded polymeric micelles.

Micelle	Polymer	Particle size (nm)	PDI
PM	PEG-*b*-P(MMA-*r*-UMA)	67.1 ± 1.61	0.168
DPM	DNP loaded PEG-*b*-P(MMA-*r*-UMA)	123.3 ± 0.92	0.153

3.4. In vitro drug release profile

DPM was successfully prepared by the dialysis method, yielding a drug loading content (DLC) of 1 wt% and a drug loading efficiency (DLE) of 9%, as determined by UV–Vis absorbance at 312 nm. The *in vitro* release profile of DNP from DPM micelles in PBS (pH 7.4, 2% Tween® 80) at 37 °C is shown in Figure 5. DNP was released in a sustained manner over 8 h, reaching nearly 100% cumulative release. Approximately 17% of the encapsulated drug was released within the first hour, followed by ~35% at 2 h and ~55% at 4 h. Thereafter, the release continued at a nearly constant rate, with ~78% released at 6 h and almost complete release by 8 h. The linear release profile suggests diffusion-controlled release of DNP from the micellar core.

This sustained yet relatively fast release behavior may be attributed to the moderate hydrophobic–hydrophilic balance of the PEG-*b*-P(MMA-*r*-UMA) copolymer, which facilitates drug solubilization while allowing efficient diffusion through the micellar shell. Such a release profile is advantageous for ensuring a rapid onset of therapeutic action while maintaining continuous drug availability over several hours.

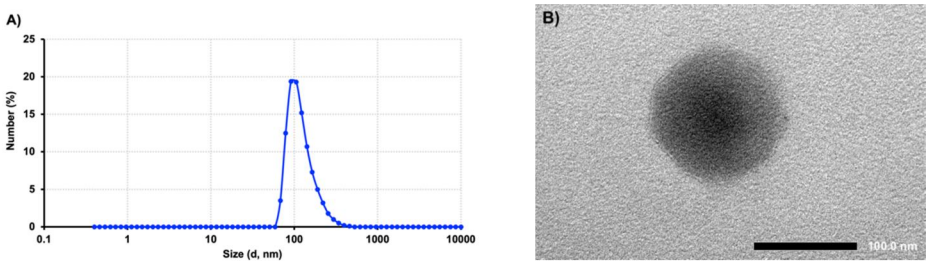

Figure 4. (a) Particle size distribution graphic and (b) transmission electron microscopy (TEM) image of DPM.

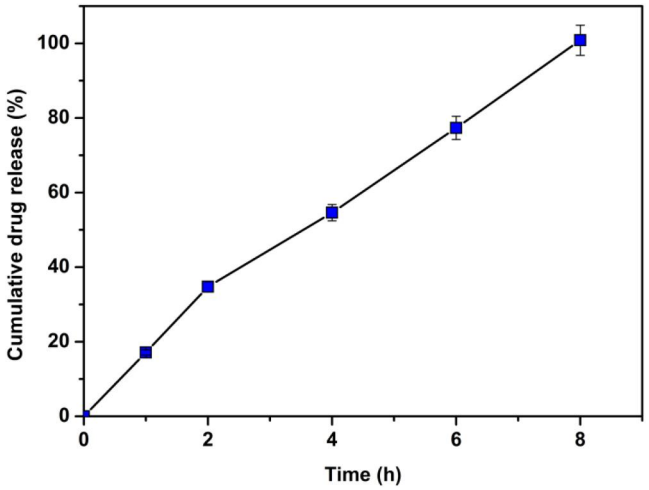

Figure 5. *In vitro* DNP release profile of DPM micelles incubated in PBS at pH 7.4 at 37°C.

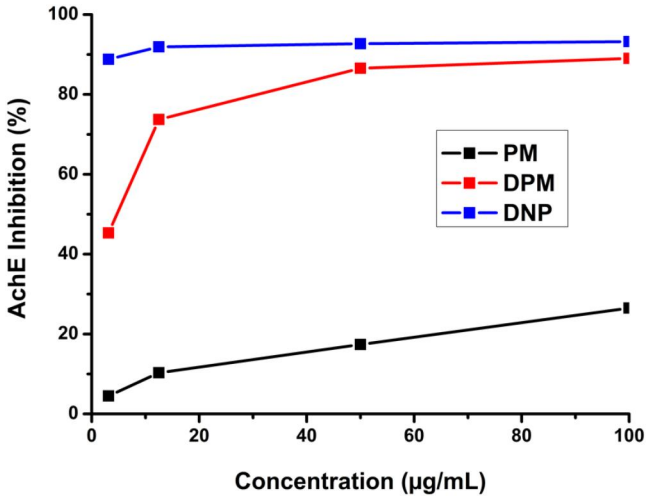

Figure 6. Acetylcholinesterase (AChE) inhibition activity of PM, DPM and DNP.

3.5. In vitro *acetylcholinesterase enzyme inhibition*

Since DNP is a clinically approved acetylcholinesterase (AChE) inhibitor used for the symptomatic treatment of AD, it was important to investigate whether drug loaded polymeric micelles retained the inhibitory activity of the free drug. Therefore, the AChE inhibitory potential of the prepared formulations was evaluated using Ellman's method, with DNP serving as the reference standard.

As shown in Figure 6, PM exhibited negligible inhibitory activity, with inhibition values remaining below 30% even at the highest tested concentration (100 µg/mL). In contrast, DPM demonstrated significant inhibition, which increased in a concentration-dependent manner. At low concentrations (10 µg/mL), DPM exhibited ~45% inhibition, which increased to ~85% at 60–100 µg/mL. Although the activity of DPM was slightly lower than that of free DNP, the inhibition profiles were nearly parallel, indicating that encapsulated drug largely retained its biological activity. The IC_{50} value of DPM was calculated as ~40 µg/mL, which is higher than that of free drug, likely due to the relatively low drug loading capacity and encapsulation efficiency (DLC = 1 wt%, DLE = 9%). These parameters, together with the IC_{50}, could be further optimized by improving drug loading strategies.

Overall, the results confirm that DNP retains its AChE inhibitory activity after encapsulation into PEG-*b*-P(MMA-*r*-UMA) micelles, while empty micelles do not contribute to enzyme inhibition. This demonstrates that the observed biological effect originates from the encapsulated DNP, supporting the potential of these polymeric micelles as effective nanocarriers for Alzheimer's therapy.

3.6. Cell viability

After 24 h incubation, the IC_{50} values of PM, DPM, and DNP were determined as 17.6 µg/mL, 8 µg/mL, and 4.2 µg/mL, respectively. These results indicate that free donepezil (DNP) exhibited the highest cytotoxicity, while PM showed the lowest cytotoxicity. Interestingly, the DPN loaded DPM demonstrated an intermediate IC_{50} value, suggesting partial masking of drug toxicity by the micelle structure.

When cell viability percentages were examined, a different trend was observed (Figure S5). While PM treatment reduced cell viability to ~30%, free donepezil maintained cell viability at ~56%. Remarkably, DPM treatment resulted in viability values exceeding 110%, suggesting a possible proliferative or protective effect associated with the micellar formulation. Statistical analysis ($p < 0.0001$) confirmed significant differences between all groups. The enhanced viability of DPM compared to both PM and DNP supports the hypothesis that the micelle structure may mitigate the cytotoxic effects of both the carrier and the drug. Similar findings have been reported for mPEG-PLA micelles, where drug loaded micelles demonstrated improved therapeutic activity and reduced systemic toxicity compared to empty micelles.[33]

A closer analysis of concentration-dependent effects further supports these observations. PM exposure (15–500 µg/mL) caused a pronounced, dose-dependent decline in viability, with survival already reduced to 60–70% at the lowest concentration tested (15 µg/mL). In contrast, DNP (0.5–17.2 µg/mL) maintained relatively high viability (~90%) at the lowest dose, but cell survival steadily declined as concentration increased, highlighting a clear toxicity threshold near its effective therapeutic range. DPM (0.26–8.5 µg/mL) showed concentration-dependent effects as well, with higher doses (8.5 µg/mL) leading to reduced viability, while lower concentrations not only preserved but in some cases enhanced viability above control levels. Statistical analysis confirmed significant differences among concentrations for each group ($p < 0.0001$) (Figure 7).

Overall, these results demonstrate that PM is intrinsically cytotoxic at relatively low concentrations, while encapsulation of DNP into micelles (DPM) both preserves drug activity and reduces toxicity of the carrier. The protective effect of micelle encapsulation may represent an advantage for therapeutic applications, offering a balance between efficacy and safety.

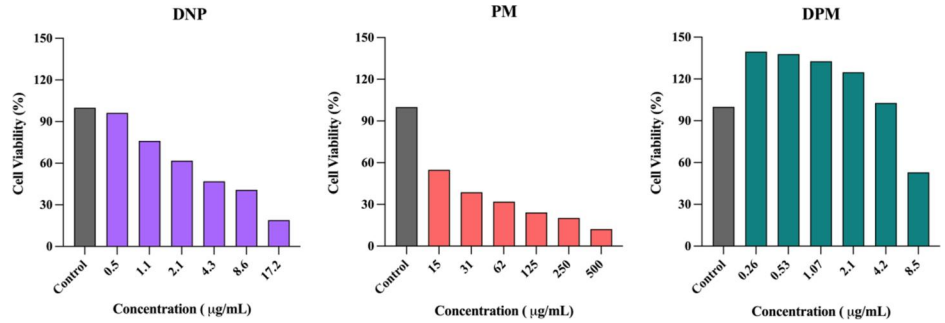

Figure 7. Cell viability (%) of SH-SY5Y cells treated with, DNP (0.5–17.2 μg/mL), PM (15–500 μg/mL), and the DPM (0.26–8.5 μg/mL). Statistical analysis using one-way ANOVA reveals significant differences between groups ($p < 0.0001$ for; PM, DNP and DPM).

4. Conclusions

In this study, uracil-functionalized amphiphilic block copolymer was synthesized *via* RAFT polymerization and successfully self-assembled into nanoscale micelles for the delivery of DNP a clinically approved acetylcholinesterase inhibitor for the treatment of AD. The design strategy relied on the incorporation of 6-methyluracil moieties into the copolymer backbone, providing additional stabilization of the micellar core through hydrogen bonding interactions. Structural characterization by FTIR, ^{1}H and ^{13}C NMR confirmed the successful synthesis of both the monomer and the copolymer, while DLS and TEM analyses revealed uniform micelle sizes, narrow dispersity, and spherical morphology. The low critical micelle concentration observed further highlighted the excellent thermodynamic stability of the micelles under physiological conditions.

DNP was successfully encapsulated into the polymeric micelles using a dialysis method, and the system demonstrated a sustained and nearly linear release profile, ensuring continuous drug availability over several hours. The drug-loaded micelles preserved the acetylcholinesterase inhibitory activity of free DNP, while the blank micelles showed negligible inhibition, confirming that the biological activity originated from the encapsulated drug. Importantly, cytotoxicity assays in SH-SY5Y cells showed that encapsulation reduced the intrinsic toxicity of both free DNP and the carrier polymer, while significantly improving cell viability. This masking effect of the micelle structure is consistent with previous studies on polymeric nanocarriers, where drug encapsulation was shown to enhance therapeutic efficacy and biocompatibility simultaneously. The results demonstrate that uracil-containing polymeric micelles represent a robust and versatile nanocarrier system for central nervous system drug delivery. Their high stability, favorable release kinetics, retention of pharmacological activity, and improved safety profile make them a promising platform for DNP delivery.

Acknowledgements

Authors acknowledge the resources and support from the Drug Application and Research Center (ILMER) at Bezmialem Vakif University.

Authors' contributions

Ayça Erkent: formal analysis, methodology, investigation, visualization, validation, writing – original draft. Gizem İğdeli: formal analysis, methodology, investigation, visualization, validation, writing – original draft. Rabia Sare Yanıkoğlu: investigation, visualization, validation, writing. Binnur Aydogan Temel: supervision, conceptualization, writing – review & editing, validation, resources, project administration, funding acquisition. All authors have read and agreed to the published version of the manuscript.

Disclosure statement

No potential conflict of interest was reported by the author(s).

Funding

A.E. thanks to the Scientific and Technological Research Council of Turkey (TUBITAK) BIDEB 2209-A University Students Research Projects Support Program (Application number: 1919B012107154) for financial support.

References

[1] Brambilla, D.; Verpillot, R.; Le Droumaguet, B.; Nicolas, J.; Taverna, M.; Kóňa, J.; Lettiero, B.; Hashemi, S. H.; De Kimpe, L.; Canovi, M.; et al. PEGylated Nanoparticles Bind to and Alter Amyloid-Beta Peptide Conformation: Toward Engineering of Functional Nanomedicines for Alzheimer's Disease. *ACS Nano*. **2012**, *6*, 5897–5908. DOI: 10.1021/nn300489k.

[2] Spillantini, M. G.; Goedert, M. Tau Protein Pathology in Neurodegenerative Diseases. *Trends Neurosci.* **1998**, *21*, 428–433. DOI: 10.1016/S0166-2236(98)01337-X.

[3] Selkoe, D. J. The Origins of Alzheimer Disease: A is for Amyloid. *JAMA*. **2000**, *283*, 1615. DOI: 10.1001/jama.283.12.1615.

[4] Helzner, E. P.; Scarmeas, N.; Cosentino, S.; Tang, M.-X.; Schupf, N.; Stern, Y. Survival in Alzheimer Disease: A Multiethnic, Population-Based Study of İncident Cases. *Neurology*. **2008**, *71*, 1489–1495. DOI: 10.1212/01.wnl.0000334278.11022.42.

[5] Xie, J.; Brayne, C.; Matthews, F. E., Medical Research Council Cognitive Function and Ageing Study Collaborators. Survival Times in People with Dementia: Analysis from Population Based Cohort Study with 14 Year Follow-up. *BMJ*. **2008**, *336*, 258–262. DOI: 10.1136/bmj.39433.616678.25.

[6] Checler, F.; Vincent, B. Alzheimer's and Prion Diseases: Distinct Pathologies, Common Proteolytic Denominators. *Trends Neurosci.* **2002**, *25*, 616–620. DOI: 10.1016/s0166-2236(02)02263-4.

[7] Cai, H.; Wang, Y.; McCarthy, D.; Wen, H.; Borchelt, D. R.; Price, D. L.; Wong, P. C. BACE1 is the Major β-Secretase for Generation of Aβ Peptides by Neurons. *Nat. Neurosci.* **2001**, *4*, 233–234. DOI: 10.1038/85064.

[8] Etienne, P.; Robitaille, Y.; Wood, P.; Gauthier, S.; Nair, N.; Quirion, R. Nucleus Basalis Neuronal Loss, Neuritic Plaques

and Choline Acetyltransferase Activity in Advanced Alzheimer's Disease. *Neuroscience.* **1986**, *19*, 1279–1291. DOI: 10.1016/0306-4522(86)90142-9.

[9] Rogers, S.; Friedhoff, L. Long-Term Efficacy and Safety of Donepezil in the Treatment of Alzheimer's Disease: An İnterim Analysis of the Results of a US Multicentre Open Label Extension Study. *Eur. Neuropsychopharmacol.* **1998**, *8*, 67–75. DOI: 10.1016/s0924-977x(97)00079-5.

[10] Herrmann, N.; Chau, S. A.; Kircanski, I.; Lanctôt, K. L. Current and Emerging Drug Treatment Options for Alzheimer's Disease: A Systematic Review. *Drugs.* **2011**, *71*, 2031–2065. DOI: 10.2165/11595870-000000000-00000.

[11] Christodoulou, C.; Melville, P.; Scherl, W. F.; MacAllister, W. S.; Elkins, L. E.; Krupp, L. B. Effects of Donepezil on Memory and Cognition in Multiple Sclerosis. *J. Neurol. Sci.* **2006**, *245*, 127–136. DOI: 10.1016/j.jns.2005.08.021.

[12] Kaur, A.; Nigam, K.; Bhatnagar, I.; Sukhpal, H.; Awasthy, S.; Shankar, S.; Tyagi, A.; Dang, S. Treatment of Alzheimer's Diseases Using Donepezil Nanoemulsion: An İntranasal Approach. *Drug Deliv. Transl. Res.* **2020**, *10*, 1862–1875. DOI: 10.1007/s13346-020-00754-z.

[13] Baysal, I.; Ucar, G.; Gultekinoglu, M.; Ulubayram, K.; Yabanoglu-Ciftci, S. Donepezil Loaded PLGA-b-PEG Nanoparticles: Their Ability to İnduce Destabilization of Amyloid Fibrils and to Cross Blood Brain Barrier in Vitro. *J. Neural Transm. (Vienna).* **2017**, *124*, 33–45. DOI: 10.1007/s00702-016-1527-4.

[14] Topal, G. R.; Mészáros, M.; Porkoláb, G.; Szecskó, A.; Polgár, T. F.; Siklós, L.; Deli, M. A.; Veszelka, S.; Bozkir, A. ApoE-Targeting İncreases the Transfer of Solid Lipid Nanoparticles with Donepezil Cargo across a Culture Model of the Blood–Brain Barrier. *Pharmaceutics.* **2020**, *13*, 38. DOI: 10.3390/pharmaceutics13010038.

[15] Quan, Peng, Guo, Wenjia, Cun, Dongmei, Yang, Mingshi, Lin Yang, Donepezil Accelerates the Release of PLGA Microparticles via Catalyzing the Polymer Degradation Regardless of the End Groups and Molecular Weights, *Int. J. Pharm.* **2023**, *632*, 122566. DOI: 10.1016/j.ijpharm.2022.122566.

[16] Rajput, A.; Butani, S. Donepezil HCl Liposomes: Development, Characterization, Cytotoxicity, and Pharmacokinetic Study. *AAPS PharmSciTech.* **2022**, *23*, 74. DOI: 10.1208/s12249-022-02209-9.

[17] Butani, S. Fabrication of an İon-Sensitive in Situ Gel Loaded with Nanostructured Lipid Carrier for Nose to Brain Delivery of Donepezil. *Asian J. Pharm. (AJP).* **2018**, *12*, 293.

[18] Suthar, T.; Jain, K. Development and Evaluation of N-Acetyl Cysteine-Grafted Polyamidoamine Dendrimers for Enhanced Brain Delivery of Donepezil Hydrochloride. *RSC Pharm.* **2025**, *2*, 1489. DOI: 10.1039/D5PM00119F.

[19] Kumar, L.; Rana, R.; Shaikh, N. K.; Thakur, A.; Kashyap, S.; Aggarwal, V.; Jyothiraditya, V. Alzheimer's Disease and Polymeric Nanocarriers: Synergistic Advances in Targeted Drug Delivery. *Curr. Top. Med. Chem.* **2025**, *25*, 2829–2847. DOI: 10.2174/0115680266347890250409153450.

[20] Haro-Martínez, E.; Muscolino, E.; Moral, N.; Duran, J.; Fornaguera, C. Crossing the Blood–Brain Barrier: Nanoparticle-Based Strategies for Neurodegenerative Disease Therapy. *Drug Deliv. Transl. Res.* **2025**. DOI: 10.1007/s13346-025-01887-9.

[21] Singh, R.; Lillard, J. W. Jr. Nanoparticle-Based Targeted Drug Delivery. *Exp. Mol. Pathol.* **2009**, *86*, 215–223. DOI: 10.1016/j.yexmp.2008.12.004.

[22] Din, F. U.; Aman, W.; Ullah, I.; Qureshi, O. S.; Mustapha, O.; Shafique, S.; Zeb, A. Effective Use of Nanocarriers as Drug Delivery Systems for the Treatment of Selected Tumors. *Int. J. Nanomed.* **2017**, *12*, 7291–7309. DOI: 10.2147/IJN.S146315.

[23] Ventola, C. L. Progress in Nanomedicine: Approved and İnvestigational Nanodrugs. *PT.* **2017**, *42*, 742–755.

[24] Alemayehu, Y. A.; Fan, W.-L.; Ilhami, F. B.; Chiu, C.-W.; Lee, D.-J.; Cheng, C.-C. Photosensitive Supramolecular Micelle-Mediated Cellular Uptake of Anticancer Drugs Enhances the Efficiency of Chemotherapy. *Int. J. Mol. Sci.* **2020**, *21*, 4677. DOI: 10.3390/ijms21134677.

[25] Avramović, N.; Mandić, B.; Savić-Radojević, A.; Simić, T. Polymeric Nanocarriers of Drug Delivery Systems in Cancer Therapy. *Pharmaceutics.* **2020**, *12*, 298. DOI: 10.3390/pharmaceutics12040298.

[26] Kaur, J.; Gulati, M.; Kapoor, B.; Jha, N. K.; Gupta, P. K.; Gupta, G.; Chellappan, D. K.; Devkota, H. P.; Prasher, P.; Ansari, M. S.; et al. Advances in Designing of Polymeric Micelles for Biomedical Application in Brain Related Diseases. *Chem. Biol. Interact.* **2022**, *361*, 109960. DOI: 10.1016/j.cbi.2022.109960.

[27] İğdeli, G.; Fritzen, L.; Pietrzik, C. U.; Temel, B. A. Preparation and Characterization of Poly (Ethylene Glycol)-b-Poly (Tert-Butyl Methacrylate) Micelles as Potential Nanocarriers for Donepezil. *Pharm. Dev. Technol.* **2024**, *29*, 1111–1120. DOI: 10.1080/10837450.2024.2423833.

[28] İğdeli, G.; Fritzen, L.; Pietrzik, C. U.; Temel, B. A. Folic Acid-Conjugated Amphiphilic Copolymers for the Enhanced Delivery of Donepezil: Synthesis, Characterization and Blood-Brain Barrier Permeability in a Co-Culture Model. *J. Biomater. Sci. Polym. Ed.* **2025**, *36*, 1882–1897. DOI: 10.1080/09205063.2025.2486863.

[29] Shishkina, S. V.; Shaposhnik, A. M.; Dyakonenko, V. V.; Baumer, V. M.; Rudiuk, V. V.; Yanchuk, I. B.; Levandovskiy, I. A. New Polymorphic Modifications of 6-Methyluracil: An Experimental and Quantum Chemical Study. *ACS Omega.* **2023**, *8*, 20661–20674. DOI: 10.1021/acsomega.3c01231.

[30] Ellman, G. L.; Courtney, K. D.; Andres, V. Jr.; Featherstone, R. M. A New and Rapid Colorimetric Determination of Acetylcholinesterase Activity. *Biochem. Pharmacol.* **1961**, *7*, 88–95. DOI: 10.1016/0006-2952(61)90145-9.

[31] Kang, Y.; Lu, A.; Ellington, A.; Jewett, M. C.; O'Reilly, R. K. Effect of Complementary Nucleobase İnteractions on the Copolymer Composition of RAFT Copolymerizations. *ACS Macro Lett.* **2013**, *2*, 581–586. DOI: 10.1021/mz4001833.

[32] Lu, Y.; Zhang, E.; Yang, J.; Cao, Z. Strategies to Improve Micelle Stability for Drug Delivery. *Nano Res.* **2018**, *11*, 4985–4998. DOI: 10.1007/s12274-018-2152-3.

[33] Wang, H.; Gong, F.; Liu, J.; Xiang, L.; Hu, Y.; Che, W.; Li, R.; Yang, S.; Zhuang, Q.; Teng, X. Engineering Docetaxel Micelles for Enhanced Cancer Therapy Through Intermolecular Forces. *Bioengineering.* **2024**, *11*, 1078. DOI: 10.3390/bioengineering11111078.